



## SWIFT-XRT-CALDB-04

Release Date: February 09<sup>th</sup>, 2012

Prepared by: Claudio Pagani, Andrew Beardmore, Tony Abbey (UL), Matteo Perri, Milvia Capalbi (ASDC)

Date revised: February 09<sup>th</sup>, 2012

Revision: 11

Revised by: Claudio Pagani & Andy Beardmore

# SWIFT-XRT CALDB RELEASE NOTE

## SWIFT-XRT-CALDB-04: Gain

### 1 Component Files

Table 1: Latest CALDB component files.

FILENAME	VALID DATE	RELEASE DATE
swxpcgains6_20010101v011.fits <sup>a</sup>	01-Jan-2001	09-Feb-2012
swxwtgains6_20010101v012.fits <sup>a</sup>	01-Jan-2001	09-Feb-2012
swxpcgains0_20010101v010.fits <sup>b</sup>	01-Jan-2001	09-Feb-2012
swxwtgains0_20010101v011.fits <sup>b</sup>	01-Jan-2001	09-Feb-2012

<sup>a</sup> 's6' refers to  $V_{ss} = 6$  V gain files. The substrate voltage was raised permanently to this value on 2007-Aug-30 at 14:25UT.

<sup>b</sup> 's0' refers to substrate voltage ( $V_{ss}$ ) 0 V gain files.

## 2 Introduction

This document contains a description of the gain calibration analysis performed at Leicester University to produce the gain calibration products for the *Swift*-XRT Calibration Database (CALDB).

Section 3 lists the changes in the *Swift* operations during the mission that had a significant impact on the gain characterisation and the modifications to the gain files and software to account for these changes. Section 4 illustrates the modifications to the gain files in this release and describes the charge traps analysis, the gain files structure, and shows the improvement in energy resolution. Appendix A describes the derivation of the gain and CTI coefficients and their implementation in the CALDB gain files; in Appendix B the gain and CTI measurements are described and Appendix C lists the previous gain file releases.

The latest XRTDAS software package, developed under the responsibility of the ASI Science Data Center (ASDC) in Italy and distributed within the HEASoft package (version 6.12, released on 2012-March-12), includes changes to the XRT analysis task XRTCALCPI to model the energy dependence of the CTI correction in the gain files with a broken power law.

## 3 Changes in Gain File release (revision 11)

Radiation damage during the orbital lifetime of *Swift* continues to degrade the XRT CCD camera performance. The interaction of soft and hard protons with the CCD produces displacements of Silicon atoms that cause charge traps in its crystal lattice, resulting in offsets in the measured photons energies and in the broadening of the spectroscopic resolution.

In September of 2007 the XRT team started a calibration program to characterise the charge losses due to traps consisting of observations of the emission line rich Cas A and Tycho Supernova Remnants (SNRs). In Photon Counting mode, the locations of the deeper traps and their depths are measured in the central 200x200 pixels of the CCD. Outside the central window, the cumulative effects of traps are evaluated for individual CCD column. Column energy offsets are also evaluated in Windowed Timing mode, that provides high time resolution with 1-D spatial localisation. The observations of the SNRs are repeated approximately every six months, and updated trap tables are derived. The CALDB gain files in this release have been updated including trap tables from 2 additional epochs (February and September 2011) as derived from observations of the Tycho SNR. Improved CALDB gain parameters characterising the energy dependence of the trap depths were derived and included in the release. By correcting for the effects of traps, a significant improvement of the FWHM of the detector is measured (see tables 2 and 3).

Analysis of the corner radioactive source data and measurements of the nickel background line has clearly shown that the CTI correction should be energy dependent. The energy dependence has been calibrated and modelled with a broken power law and is included in the current gain CALDB release.

The XRTCALCPI software task and the gain files format have been modified to implement the energy corrections for charge traps and the CTI energy dependence. The software will automatically apply the appropriate gain corrections dependent on the time of observation, temperature

and event position. The trap mapping analysis, the new gain files formats and the relevant software updates are described in detail in the following section.

The loss of the CCD active cooling system shortly after launch forced the instrument to rely on passive cooling provided by the XRT radiator in order to operate the detector in the  $-75^{\circ}\text{C}$  to  $-50^{\circ}\text{C}$  temperature range rather than the  $-100^{\circ}\text{C}$  envisaged before launch. The main effect of operating at such temperatures is a significant level of dark current and elevated CCD noise at low energies, with an increasing number of hot and ‘flickering’ pixels at higher temperatures.

On 2007-Aug-30 at 14:25UT, the XRT team performed a planned substrate voltage ( $V_{ss}$ ) change from 0 V to 6 V in order to reduce the thermally induced dark current when the operating temperature is above  $-55^{\circ}\text{C}$ . Prior to the change, preliminary observations of Cas A and the Crab at a  $V_{ss}$  of 6 V showed a reduction in the Quantum Efficiency of the order of 10% at 6 keV (Godet et al. 2007, SPIE, 6686) and an increase of about 5% in the gain due to the change in the gain of the output FET. The latter meant separate gain files are needed depending on the substrate voltage at the time of a given observation. The files are distinguished using the notation *s0* (for  $V_{ss} = 0$  V) and *s6* (for  $V_{ss} = 6$  V) in their respective file names. The *Swift* software tools were updated to perform a query for the relevant gain file to be used depending on the substrate voltage setting.

In addition to the substrate voltage change, in 2008 June, after successful XRT flight software updates, the XRT CCD began permanently operating in full frame Photon Counting mode (‘pcw3’), whereby the entire  $600 \times 600$  imaging area of the CCD is read out. This has enabled us to continuously collect corner source  $^{55}\text{Fe}$  calibration data (see figure A.1) when operating in photon counting mode and has provided us with a wealth of information on the gain and charge transfer efficiency (CTE) behaviour as a function of time and CCD temperature since this time.

This latest CALDB release (2012-Feb-09) includes new versions of the  $V_{ss} = 6$  V gain files, with updated identification of trap locations and depths derived from Tycho SNR observations in February and September 2011 and improved gain coefficients to characterise the trap depths energy dependence for both Photon Counting (PC) mode (**swxpcgains6\_20010101v011.fits**) and Windowed Timing (WT) mode (**swxwtgains6\_20010101v012.fits**).

The updated XRTDAS software version 2.8.0 implements the modelling of the energy dependence of the CTI corrections (coefficients GC1 and GC2 of the gain files) with a broken power law. The ‘Calibration Dataset Codename’, used by the software to query the CALDB has been set to ‘GAIN2’ in the new gain files:

CCNM0001= ‘GAIN2 ’ / Type of Calibration data

This setting prevents the software from using an incorrect version of the gain files.

The CALDB release also includes a new version of the PC and WT  $V_{ss} = 0$  V gain files: (**swxpcgains0\_20010101v010.fits** and **swxwtgains0\_20010101v011.fits**), with the Dataset Codename CCNM0001 set to ‘GAIN2’, to be used by the new software in case of a substrate voltages change.

## 4 Gain file creation

### 4.1 Introduction

The CALDB gain files format has been substantially modified in the previous release to allow for the energy correction for charge trap losses. The traps are identified in the gain files by their locations in detector coordinates (RAWX, RAWY), their extensions in pixels (YEXTENT) and their depths in eV (OFFSET) measured at the incident photons reference energy of 1.856 keV (the observed Cas A Silicon  $K\alpha$  energy).

In the current release the gain parameters used to describe the energy dependence of the trap depths, modelled with a broken power law, have been updated. The new coefficients provide improved fits of the emission lines of the E0102, Cas A and Tycho SNRs.

The gain files include coefficients for the gain and the parallel and serial CTI for different epochs at three reference CCD temperatures (-75C, -65C and -48C). The coefficients are derived using the  $^{55}\text{Fe}$  line in the corner sources spectra at different epochs. Two sets of gain and CTI coefficients are included in the gain files for this release. One set of coefficients, derived from all the events in the corner sources, is used by the software to calculate the event energy when no trap correction is applied. The second set, derived from the columns of the corner sources less affected by charge traps, is used when the traps energy corrections are applied. The modelling of the CTI energy dependence was changed to a broken power-law functional form:

$$\begin{aligned} CTI(E) &= CTI(E_{55\text{Fe}}) \left(\frac{E}{E_{55\text{Fe}}}\right)^{-\beta_1} & (E \leq E_{55\text{Fe}}) \\ &= CTI(E_{55\text{Fe}}) \left(\frac{E}{E_{55\text{Fe}}}\right)^{-\beta_2} & (E > E_{55\text{Fe}}) \end{aligned}$$

The derived  $\beta_1$  and  $\beta_2$  parameters for PC and WT mode provide good fits to the SNR observations. The new version of the task XRTCALCPI correctly interprets the updated parameters of the gain files to implement the broken power-law energy dependence of the CTI. The details of the gain and CTI coefficients measurements are described in Appendix A.

Starting with the release HEASOFT 6.11, the *Swift* software derives the trap corrected energy and saves it in the *PI* column of the cleaned events files for each valid X-ray event. Optionally, the user can also save two additional columns corresponding to the energy correction applied (*PI\_OFFSET*) and the uncorrected energy (*PI\_NOM*) of each event using the optional parameters *savepinom* and *savepioffset* of the XRTCALCPI task. By default, spectra are extracted in XSELECT from the *PI* values. The user can extract spectra of uncorrected events energies using the XSELECT command *set phaname PI\_NOM*.

Photon Counting trap corrected spectra extracted using the new version 11 of the PC gain file (**swxpcgains6\_20010101v011.fits**) should be fitted with the newly released PC RMF+ARF version 13 (**swxpc0to12s6\_20010101v013.rmf** and **swxpc0s6\_20010101v013.rmf**, **swxpc0to12s6\_20010101v013.arf** and **swxpc0s6\_20010101v013.arf**). Windowed Timing trap corrected spectra extracted using the new version 12 of the WT gain file (**swxpcgains6\_20010101v012.fits**) should be fitted with the WT RMF+ARF version 14 (**swxwt0to2s6\_20010101v014.rmf** and **swxwt0s6\_20010101v014.rmf**, **swxwt0to2s6\_20010101v014.arf** and **sw-**

Cas A spectral degradation 2005 vs 2010

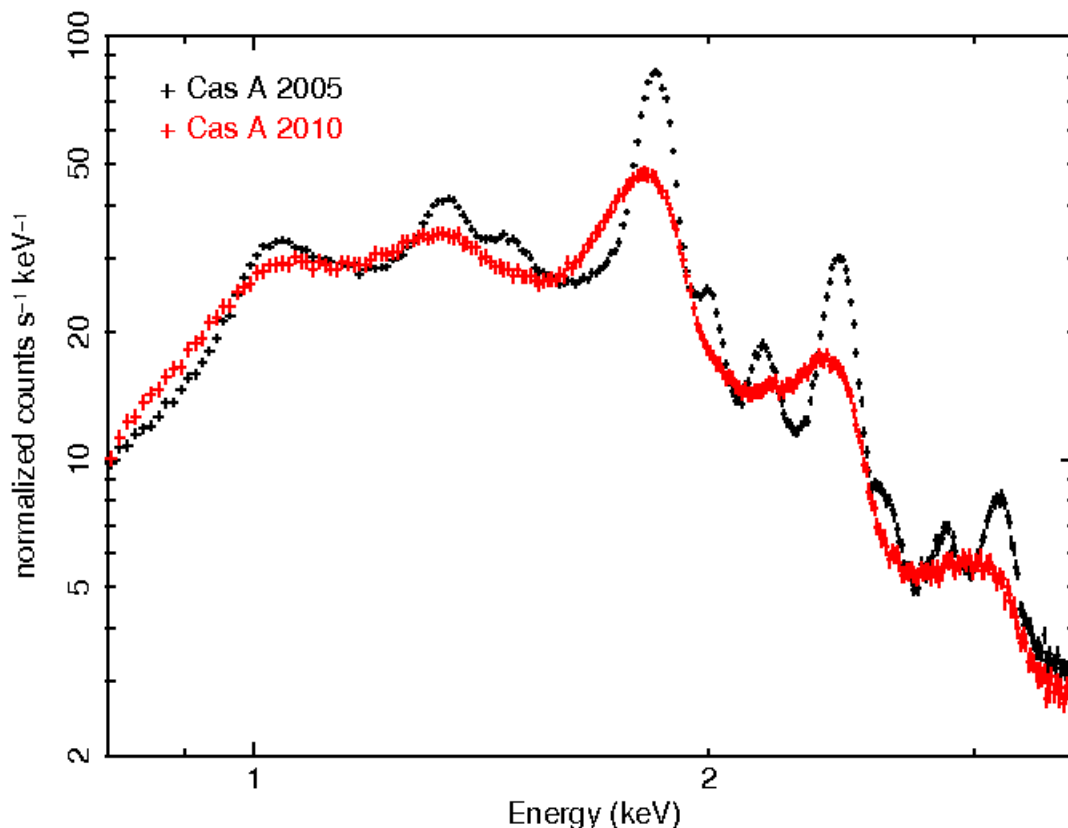


Figure 1: Comparison of the Windowed Timing mode Cas A spectrum at launch and in a recent 2010 observation, showing the reduced energy resolution that causes the broadening of the brighter lines of the remnant and the complete disappearance of the weaker lines. The fit of the Silicon K  $\alpha$  line with an asymmetric Gaussian in IDL yielded an FWHM of  $103 \pm 3$  eV and of  $259 \pm 37$  eV, in the 2005 and 2010 dataset respectively.

xwt0s6\_20010101v014.arf ).

## 4.2 Trap mapping

The extreme *Swift* environment, and in particular the transits through the South Atlantic Anomaly, have caused a substantial degradation of the CCD performance, mostly due to the creation of charge traps. Figure 1 shows the comparison of the Cas A SNR spectrum at launch and in an observation taken in 2010. The energy degradation is severe, causing the broadening of the brighter lines and the disappearance of the weaker ones.

The initial approach in dealing with the spectral degradation had been the application of a broadening function to the original spectral response. Using this technique the XRT team generated and released RMFs<sup>a</sup> with a redistribution function which matches the broadened

<sup>a</sup>Two sets of WT and PC RMFs including an epoch-dependent broadened kernel have been released: the first set should be used for data collected from 2007 March 1 to 2007 August 31 (swxpc0to12s0\_20070301v011.rmfm & swxpc0s0\_20070301v011.rmfm for PC mode and swxwt0s0\_20070301v011.rmfm & swxwt0to2s0\_20070301v011.rmfm for WT mode) the second set from 2007 September 01 onwards (swxpc0to12s6\_20070901v011.rmfm & swxpc0s6\_20070901v011.rmfm for PC mode

response kernel of the detector at any time. As the spectral resolution continued to worsen, this temporary fix was replaced by the more accurate approach of mapping the locations and depths of the traps and correcting the event data for the energy losses incurred. The benefit of this method is that it can potentially restore the spectral resolution of the CCD to something approaching its value at launch.

The calibration targets chosen for the traps mapping observations are the Cas A and Tycho SNRs, as they are constant, extended X-ray sources and have strong Silicon  $K\alpha$  emission lines that can be used as a reference energy. The first attempts at trap mapping in 2007 involved a series of  $8 \times 15$  ks observations of Cas A at various offsets pointings. More recently the Tycho SNR was chosen because of its larger size compared to the Cas A SNR, thus requiring a reduced exposure time.

#### 4.2.1 Photon Counting mode trap mapping

In Photon Counting mode traps are mapped in the central 200x200 pixels window of the CCD, where most of the GRB afterglows and other astrophysical X-ray sources are observed by the XRT. The exact trap localisation ideally requires the collection of enough source events to fit the Si- $K\alpha$  line with a Gaussian for each CCD pixel. This isn't feasible, as it would greatly exceed the allocated calibration observing time of the *Swift* mission. In practice, the exposure times of the Cas A and Tycho calibration observations are sufficient to obtain an acceptable Gaussian fit of the Si- $K\alpha$  line from the merging of events of 20 adjacent pixels. Software tools have been developed to fit the Si- $K\alpha$  line along the CCD columns, to localise traps and measure their depths. An example of trap mapping and correction is shown in Figure 2. A trap  $\simeq 100$  eV deep is localised in Column DETX = 256, at the approximate row coordinate DETY = 310. In the top plot, each datapoint is the energy centroid of the Gaussian fit of events collected in the 20 pixels above the DETY row coordinate. The line centroid energy after the correction for trap losses has been applied is shown in the bottom plot. This technique allows the identification of traps with a depth of 20 eV or larger.

Figure 3 is the comparison of the spectrum of the Tycho remnant observed in October 2009 and the spectrum after the correction for traps has been applied, showing an evident recovery of the spectral lines and of the energy resolution. To quantify the improvement in resolution the Si- $K\alpha$ , S- $K\alpha$  and Fe- $K\alpha$  lines of the observed and the corrected spectra of different calibration epochs were fitted in IDL with an asymmetric Gaussian. The results are reported in Table 2.

Trap mapping of the central window of the CCD requires a substantial investment of observing time. Outside the central 200x200 pixels, to keep the exposure time within the allocated calibration time budget, shorter observations of the SNRs are collected, allowing the measurement of the cumulative charge losses due to traps in specific columns (columns energy offsets). This approach, that doesn't localise and correct for the charge losses of individual traps, provides nevertheless a considerable improvement of the energy resolution.

The serial CTI coefficient is defined as the fraction of charge lost per pixel during serial transfers. In reality, the CTI is not uniform over the detector because of the non-uniform distribution of traps. The measurement of the columns energy offsets is in effect a more precise characterisation of the serial charge losses than the CTI coefficient, because it evaluates the charge lost for each column. Hence, the serial CTI coefficient GC1\_TRAP has been set to zero in the current release.

and `swxwt0s6_20070901v012.rmf` & `swxwt0to2s6_20070901v012.rmf` for WT mode)

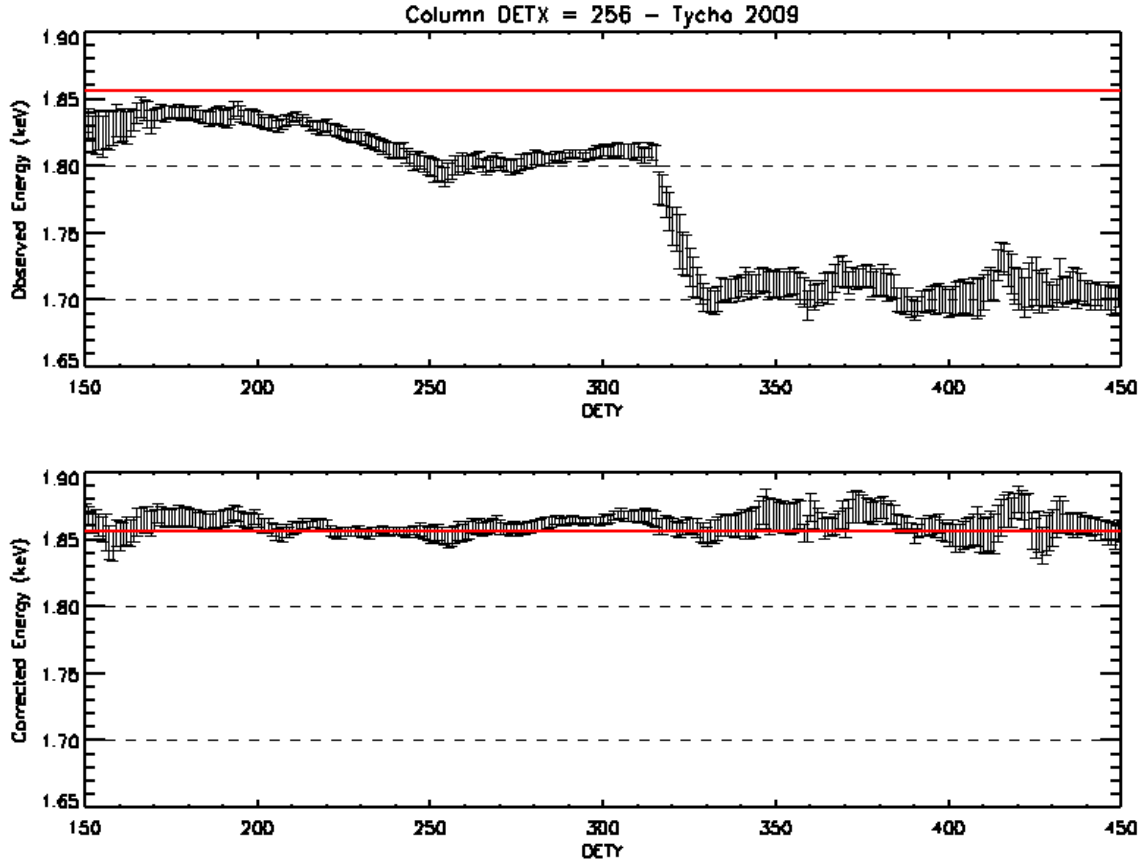


Figure 2: In the top plot, a deep trap is identified in a Cas A Photon Counting mode observation in CCD column DETX=256 at DETY  $\sim$  310; in the bottom plot, the Si-K $\alpha$  line energy is restored after the trap correction has been applied.

#### 4.2.2 Windowed Timing mode trap mapping

Windowed Timing mode provides high time resolution with 1-D spatial localisation, therefore it is not possible to measure the row coordinates and depths of single traps. For this reason, global energy offsets from the reference Si-K $\alpha$  line are measured on a column by column basis, as in PC observations outside the central 200x200 pixels window.

The *Swift-XRT* pipeline can estimate the *average* row coordinate of a source observed in WT mode if the Right Ascension and the Declination of the target are specified when processing the data. To take advantage of the estimated source average row coordinate for trap mapping purposes, in the latest round of calibration observations Tycho was observed in WT mode at three offsets pointings, at the average CCD row positions DETY=100, DETY=300 and DETY=500, allowing the derivation of the energy offsets of three segments of each column (from DETY=[1,200], DETY=[201,400] and DETY=[401,600]). It is therefore recommended to specify the target's RA and Dec when running the *Swift-XRT* pipeline to obtain the best possible energy resolution in Windowed Timing mode.

Table 3 reports the FWHM values of the Si-K $\alpha$ , S-K $\alpha$  and Fe-K $\alpha$  lines of the observed and the corrected spectra at different epochs, fitted in IDL with an asymmetric Gaussian. Figure 4 compares the observed and corrected WT spectra of Cas A taken in October of 2007.

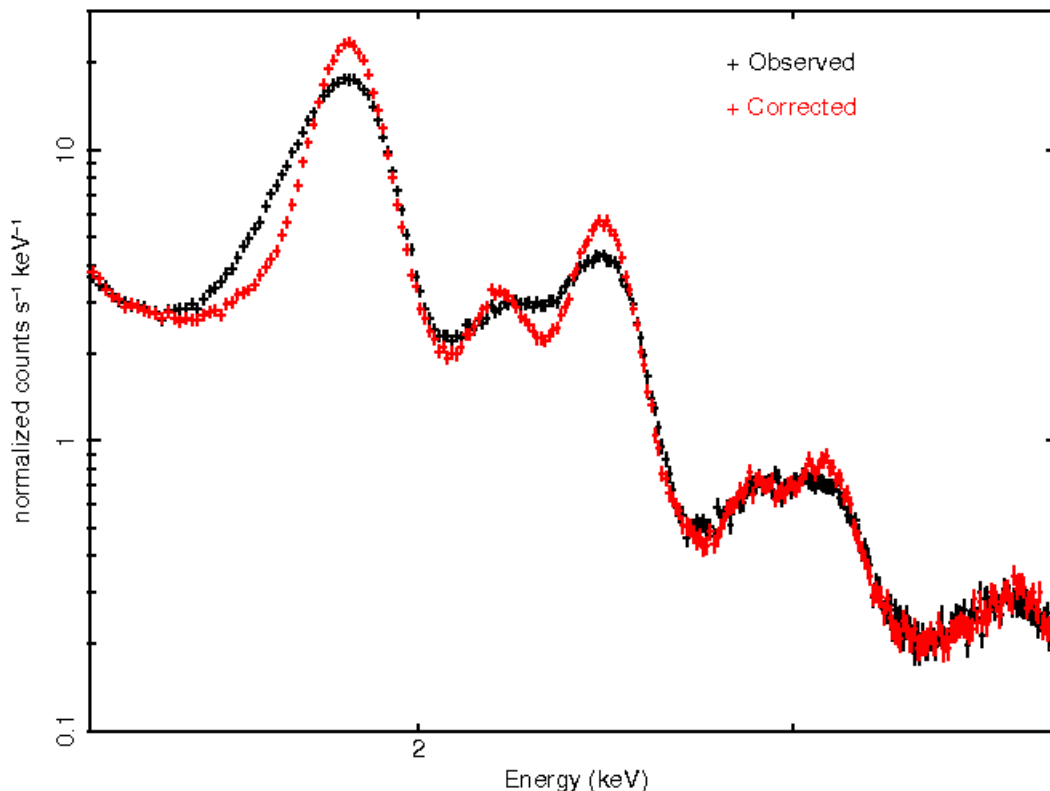


Figure 3: Comparison of the observed and the trap corrected spectra extracted from a PC mode observation of the Tycho SNR from October 2009. The fit of the Silicon  $K\alpha$  line with an asymmetric Gaussian in IDL yielded a FWHM of  $179 \pm 8$  eV for the observed spectrum and of  $132 \pm 3$  eV for the corrected spectrum.

#### 4.2.3 Energy dependence

The traps energy offset is a function of the incident photon energy. The energy dependence is modelled in the gain files with a broken power law.

$$\begin{aligned} \text{Offset}(E) &= \text{Offset}(E_{\text{break}}) \left( \frac{E}{E_{\text{break}}} \right)^{\alpha_1} & (E \leq E_{\text{break}}) \\ &= \text{Offset}(E_{\text{break}}) \left( \frac{E}{E_{\text{break}}} \right)^{\alpha_2} & (E > E_{\text{break}}) \end{aligned}$$

The Sulfur and Iron lines in Cas A and Tycho are used to derive the energy dependence above the break, while observations of the SNR E0102 with emission lines between 0.5 and 1 keV were used below the break. In the previous version of the gain files the break was set at the reference energy of 1.856 keV, at which the trap depths were derived. The reanalysis of the E0102, Tycho and Cas A SNRs datasets revealed improved fits to the emission lines when the break was set to 3.0 keV in WT mode observations. The observed and trap-corrected spectrum of the SNR E0102 used for this analysis is shown in Figure 5. PC mode observations yielded  $\alpha_1 = 0.80$  and  $\alpha_2 = 0.80$ ; for WT mode observations before 2011, the measured slopes are  $\alpha_1 = 0.70$  and  $\alpha_2 = 0.50$ , since 2011 the slopes are  $\alpha_1 = 0.80$  and  $\alpha_2 = 0.50$ .

Table 2: PC spectral resolution: Full width half maximum (FWHM) in eV of the Silicon, Sulfur and Iron  $K\alpha$  lines of the observed and the corrected spectra at different calibration epochs (specified as YYYY/MM). The FWHM values at Sulfur and Iron are only reported when enough counts in the lines allow for a reliable fit.

Source	Epoch	Line	$FWHM_{observed}$	$FWHM_{corrected}$
CasA	2007/09	Si	$138 \pm 7$	$114 \pm 2$
		S	$200 \pm 11$	$146 \pm 6$
		Fe	$318 \pm 22$	$286 \pm 21$
CasA	2009/02	Si	$154 \pm 8$	$122 \pm 2$
		S	$251 \pm 18$	$163 \pm 7$
		Fe	$372 \pm 25$	$321 \pm 14$
Tycho	2009/10	Si	$179 \pm 8$	$132 \pm 3$
		S	$267 \pm 14$	$182 \pm 8$
		Fe	$381 \pm 45$	$299 \pm 31$
Tycho	2010/03	Si	$177 \pm 7$	$138 \pm 3$
		S	$256 \pm 10$	$184 \pm 8$
		Fe	$381 \pm 39$	$307 \pm 32$
Tycho	2010/10	Si	$192 \pm 7$	$139 \pm 7$
		S	$269 \pm 11$	$192 \pm 11$
		Fe	$387 \pm 34$	$304 \pm 27$
Tycho	2011/02	Si	$185 \pm 6$	$143 \pm 7$
Tycho	2011/09	Si	$191 \pm 7$	$147 \pm 7$

Table 3: WT spectral resolution: Full width half maximum (FWHM) in eV of the Silicon, Sulfur and Iron  $K\alpha$  in the observed and the the corrected spectra for different calibration epochs (specified as YYYY/MM). The FWHM values at Sulfur and Iron are only reported when enough counts in the lines allow for a reliable fit.

Source	Epoch	Line	$FWHM_{observed}$	$FWHM_{corrected}$
CasA	2007/10	Si	$152 \pm 13$	$106 \pm 3$
		S	$244 \pm 15$	$138 \pm 7$
		Fe	$383 \pm 16$	$304 \pm 15$
CasA	2008/07	Si	$157 \pm 14$	$113 \pm 4$
		S	$274 \pm 17$	$154 \pm 9$
		Fe	$393 \pm 22$	$325 \pm 17$
CasA	2009/10	Si	$212 \pm 16$	$120 \pm 3$
		S	$302 \pm 11$	$170 \pm 11$
Tycho	2009/11	Si	$222 \pm 15$	$136 \pm 7$
Tycho	2010/10	Si	$238 \pm 12$	$148 \pm 5$
Tycho	2011/02	Si	$234 \pm 11$	$150 \pm 6$
Tycho	2011/08	Si	$249 \pm 12$	$154 \pm 6$

Cas A 2007 WT mode – Observed and Corrected Spectra

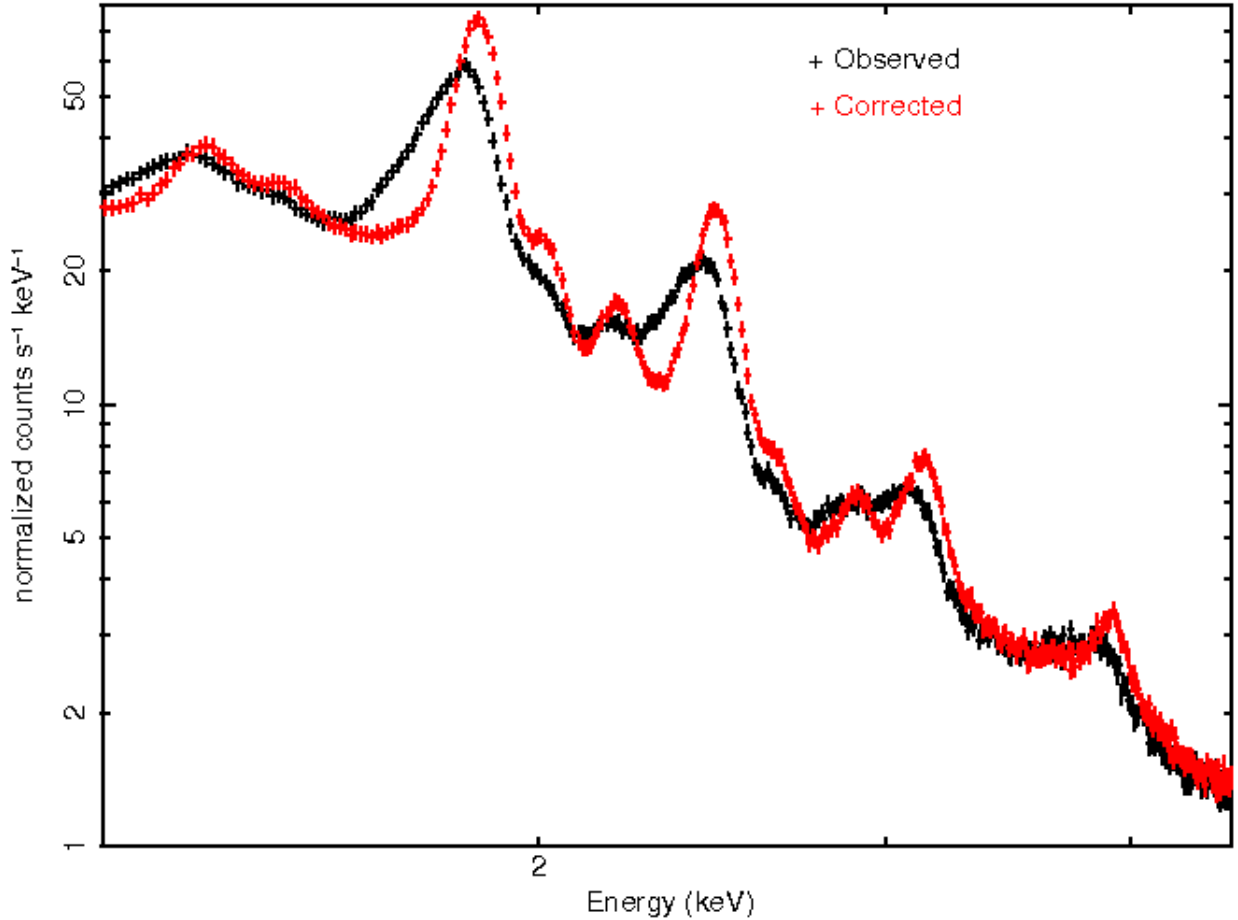


Figure 4: Comparison of the observed and the trap corrected spectra extracted from WT observations of the Cas A SNR in October of 2007. The fit of the Silicon  $K\alpha$  line with an asymmetric Gaussian in IDL yielded a FWHM of  $152 \pm 13$  eV for the observed spectrum and of  $106 \pm 3$  eV for the corrected spectrum.

### 4.3 Quality of the new gain files

This release include gain files with updated trap measurements from the two most recent calibration epochs, February and August-September 2011. The February 2011 observations showed no significant additional radiation damage since the previous October 2010 calibration epoch, as the spectra are appropriately trap-corrected by the current version of the gain files, that produce line centroids at the expected energies and FWHMs comparable to the October 2010 epoch. On the contrary, the August-September 2011 observations showed that additional damage had occurred. Figure 6 compares the spectra in October 2010 and August-September 2011. The additional damage is particularly evident in the WT mode dataset (right panel, red spectrum), that presents line centroids shifts of 30-40 eV compared to the expected energy values when extracted using the current version of the gain file. Newly derived trap measurements included in this release are necessary to restore the remnant lines at the correct energies (green spectrum).

The implementation of the energy correction for the charge lost due to deep traps and the in-

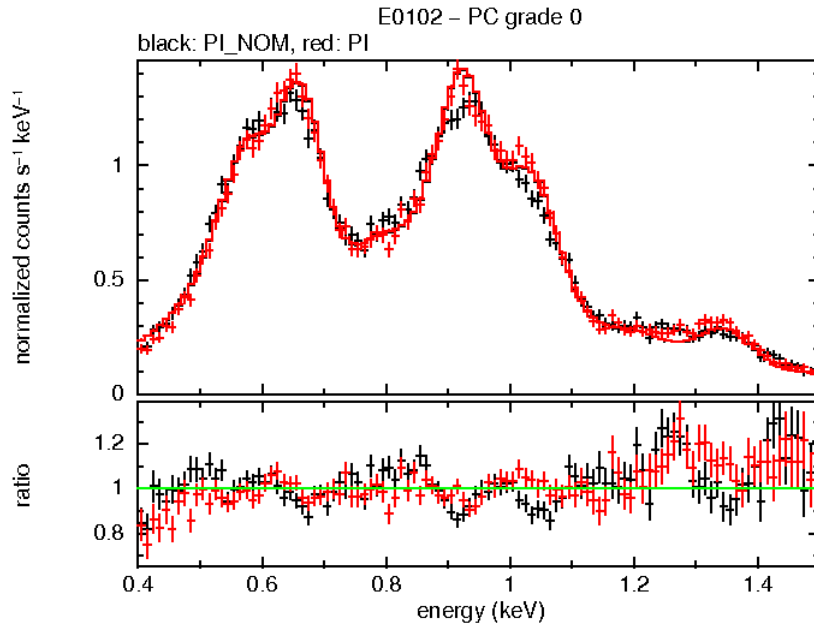


Figure 5: Observed (black) and trap-corrected (red) spectrum of E0102 used to determine the CTE energy dependence at low energies. Dataset from 2008 to 2010 were merged to extract the spectra, and grade 0 events were selected. There is a definite improvement of the lines around 0.675, 0.915 and 1.035 keV in the trap corrected spectrum.

clusion of the CTI energy dependence provide a significant improvement over the non-corrected spectra extracted with the previous versions of the gain files. The substantial recovery of the energy resolution of the trap-corrected spectra is summarised in tables 2 and 3 for calibration observations of Cas A and Tycho of different epochs. Spectra of bright sources like Mrk 421 show an improvement in the residuals close to the instrumental edges (Oxygen and Silicon) when the trap correction is applied.

This release also improves the characterisation of the energy dependence of the trap depths, modelled with a broken power law. In particular, the newly derived break energy and the power law indices in WT mode provide more accurate energy centroids at the Sulfur and Iron lines in Cas A and Tycho and lower energy lines in E0102.

Some limitations remain in the current release. The accuracy of the trap mapping measurements in Photon Counting mode data is dependent on the statistics of the reference Silicon  $K\alpha$  line, and only traps with a depth greater than 20 eV can be identified; the effects of shallower traps are included in the general CTI description. Outside the central 200x200 pixel window columns energy offsets are used to correct the data, but deep traps can cause energy shift that remain unaccounted for. Moreover, the analysis of the corner source data has shown that the traps depth is a function of the CCD temperature (the likely cause is that the dark current partially fills the traps, thus at higher CCD temperatures less charge is lost during the transfers) but at this time the temperature dependence is not modelled in the gain file. Finally, in WT mode observations, traps are not mapped individually, and only the cumulative energy offsets of each column is measured and corrected for.

Because of the mentioned limitations and the intrinsic non uniformity of the distribution of traps on the detector a general description of the accuracy of the XRT energy scale for this gain file calibration release is not straightforward. We estimate the accuracy by fitting short

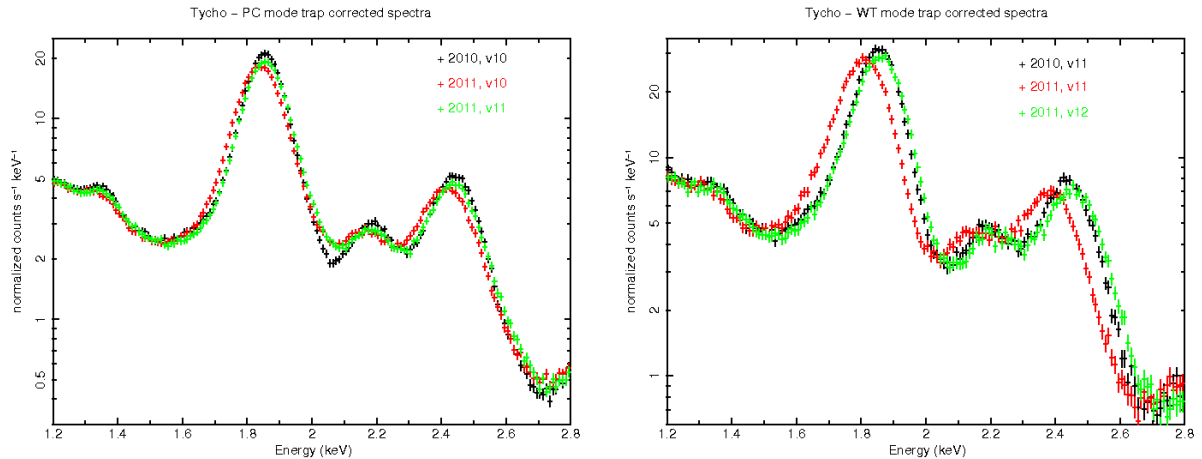


Figure 6: Evidence of recent radiation damage in the August-September 2011 observations. Left panel: Tycho PC mode spectra from October 2010 (in black) and September 2011 (in red and green). The September 2011 spectrum (in red) extracted with the current version 10 of the gain file is shifted to lower energies because of additional radiation damage. The new version 11 gain file process and corrects the data with up-to-date trap measurements, restoring the emission lines at the expected energies (green spectrum). Right panel: WT mode observations in October 2010 and August 2011, with the additional damage causing an even larger spectral shift.

observations of the Cas A SNR taken months after the trap-mapping calibration epochs using XMM derived models. When the line energies are left as free parameters of the fit differences of less than 10 eV from the XMM values are measured in the PC spectrum, while in WT mode the differences are higher, up to 26 eV at Iron.

## APPENDIX

### A Gain and CTI coefficients

#### A.1 Introduction

The charge transfer efficiency ( $CTE$ ) is defined as the fractional charge lost per pixel during the charge transfer process. So after  $N$  transfers the remaining charge  $Q$  is

$$Q = Q_o(CTE)^N \quad (\text{A.1})$$

where  $Q_o$  is the initial charge. Or in terms of charge transfer inefficiency  $CTI = 1 - CTE$  this is just

$$Q = Q_o(1 - CTI)^N \quad (\text{A.2})$$

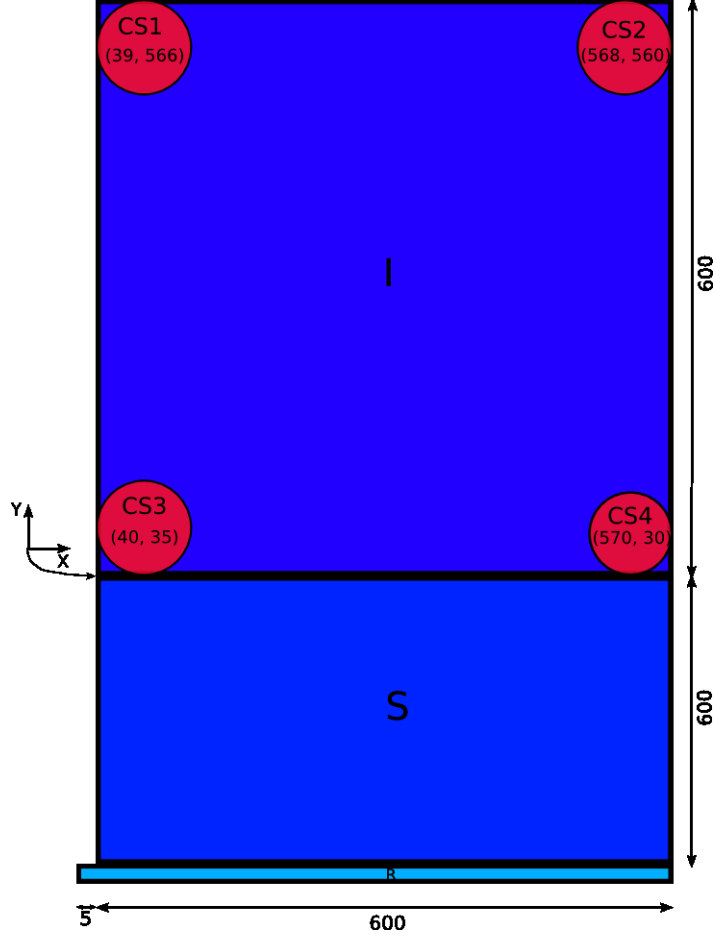


Figure A.1: Schematic of the *Swift*-XRT CCD22 identifying the imaging (I) and frame-store (S) sections, the readout register (R), and the  $^{55}\text{Fe}$  corner sources (CS). Charged is clocked in the parallel direction (Y), through both the imaging and frame-store sections, which have charge transfer inefficiencies  $CTI_{p,i}$  and  $CTI_{p,f}$ , respectively, and in the serial direction through the readout register with  $CTI_s$ .

## A.2 Event energy measured in the SWIFT-XRT CCD22

A schematic of the *Swift*-XRT CCD22 is showed in figure A.1. When an incident X-ray of energy  $E$  is registered as an event at a detector position  $(X, Y)$  in the image section it suffers charge loss from  $Y$  transfers in the parallel direction through the image section, from  $Y_S = 600$  transfers in the parallel direction through the frame-store section and from  $X + 5$  transfers in the serial direction through the readout register (+5 as there are 5 additional pixels at the end of the readout register). In order to describe the total charge lost effectively we need separate  $CTI$  coefficients for the parallel transfer losses incurred in the image and frame-store sections ( $CTI_{p,i}$  and  $CTI_{p,f}$ , respectively, as the physical volume of the pixels are smaller in the latter compared with the former) and another for the serial transfer losses ( $CTI_s$ ).

The event is registered by the ADC as a pulse-height analysed digital number  $D$  (i.e. the *PHA* value) according to the following:

$$D = \frac{E}{A} (1 - CTI_{p,i})^Y (1 - CTI_{p,f})^{Y_S} (1 - CTI_s)^{(X+5)} \quad (\text{A.3})$$

Or rearranging slightly, this becomes

$$\begin{aligned}
D &= E \left[ \frac{(1 - CTI_{p,f})^{Y_s} (1 - CTI_s)^5}{A} \right] (1 - CTI_{p,i})^Y (1 - CTI_s)^X \\
&= \frac{E}{A'} (1 - CTI_{p,i})^Y (1 - CTI_s)^X
\end{aligned} \tag{A.4}$$

where  $A' = A / ((1 - CTI_{p,f})^{Y_s} (1 - CTI_s)^5)$  is the system gain.

### A.3 CTI coefficients

The parallel CTI can be determined from CS3 and CS1 by using equation A.4 to construct the ratio  $(D_3 - D_1)/D_3$ , where  $D_n$  are the measured  $^{55}\text{Fe}$  central energies (in DN) for source  $n = 1 \dots 4$ , which is

$$\begin{aligned}
\frac{D_3 - D_1}{D_3} &= \frac{(1 - CTI_{p,i})^{Y_3} (1 - CTI_s)^{X_3} - (1 - CTI_{p,i})^{Y_1} (1 - CTI_s)^{X_1}}{(1 - CTI_{p,i})^{Y_3} (1 - CTI_s)^{X_3}} \\
&= 1 - (1 - CTI_{p,i})^{(Y_1 - Y_3)} (1 - CTI_s)^{(X_1 - X_3)}
\end{aligned} \tag{A.5}$$

$$= 1 - (1 - CTI_{p,i})^{(Y_1 - Y_3)} \tag{A.6}$$

where equation A.6 is a simplification assuming  $X_1 \approx X_3$  for transfers dominating in the parallel direction (i.e.  $Y_1 - Y_3 \gg X_1 - X_3$ ). Rearranging we find

$$CTI_{p,i} = 1 - \left( \frac{D_1}{D_3} \right)^{1/(Y_1 - Y_3)} \tag{A.7}$$

We often make use of the small number approximation (i.e.  $(1 + x)^n \approx 1 + nx$ ) so equation A.6 becomes

$$\frac{D_3 - D_1}{D_3} = (Y_1 - Y_3) CTI_{p,i}$$

That is, the parallel CTI is

$$CTI_{p,i} = \frac{D_3 - D_1}{D_3(Y_1 - Y_3)} \tag{A.8}$$

A similar equation can be derived for the parallel CTI derived from CS4 and CS2.

Likewise, the serial CTI can be shown to be

$$CTI_s = 1 - \left( \frac{D_4}{D_3} \right)^{1/(X_4 - X_3)} \tag{A.9}$$

$$= \frac{D_3 - D_4}{D_3(X_4 - X_3)} \tag{A.10}$$

## A.4 Gain

We can obtain the gain  $A'$  from CS3, which is the corner source closest to the output amplifier,

$$A' = \frac{E_{55\text{Fe}}}{D_3} (1 - CTI_{p,i})^{Y_3} (1 - CTI_s)^{X_3} \quad (\text{A.11})$$

where  $E_{55\text{Fe}} = 5895.45$  eV,  $X_3 = 40$  and  $Y_3 = 35$ . Note the term  $(1 - CTI_{p,i})^{Y_3} (1 - CTI_s)^{X_3}$  which provides a small correction to the simple gain estimate of  $E_{55\text{Fe}}/D_3$  and ensures the event energy is calculated relative to the origin  $(0, 0)$  of the imaging section of the CCD.

## A.5 Comparison with the CALDB gain file

The CALDB gain file defines the *PHA* channel to *PI* channel conversion as

$$PI \times G = PHA (GC0 + X \times GC1 + Y \times GC2) + GC3 + X \times GC4 + Y \times GC5 \quad (\text{A.12})$$

where  $GCn$  are the gain file coefficients (which are interpolated over time and CCD temperature), and  $G = 10$  eV is the nominal gain.

Equation A.4 can be rearranged to give the event energy from the measured DN value, assuming the *CTI* coefficients are known,

$$E = A' D (1 - CTI_{p,i})^{-Y} (1 - CTI_s)^{-X}. \quad (\text{A.13})$$

Note, this is the exact form of the equation required to reconstruct the event energy from the measure DN value, knowing the gain ( $A'$ ) and *CTI* values.

This equation can be made to resemble the CALDB formula by using the small value approximation expansion :

$$\begin{aligned} E &= A' D (1 + Y CTI_{p,i}) (1 + X CTI_s) \\ &= A' D (1 + X CTI_s + Y CTI_{p,i} + X Y CTI_s CTI_{p,i}) \end{aligned}$$

and dropping the last negligibly small term to give

$$\begin{aligned} E &= A' D (1 + X CTI_s + Y CTI_{p,i}) \\ &= D \{A' + X (A' CTI_s) + Y (A' CTI_{p,i})\}. \end{aligned} \quad (\text{A.14})$$

By comparison with equation A.12, we see that

$$\begin{aligned} GC0 &= A' \\ GC1 &= A' CTI_s \\ GC2 &= A' CTI_{p,i} \end{aligned} \quad (\text{A.15})$$

In practise,  $CTI_s$  is estimated from corner sources CS3–CS4, while  $CTI_{p,i}$  is estimated as the average parallel CTI from corner sources CS1–CS3 and CS2–CS4.

The term  $GC3$  in equation A.12 represents an offset (in eV) associated with the readout electronics.

## A.6 CTI coefficients energy dependence

Laboratory experiments and various X-ray missions (e.g. Chandra, Suzaku) indicate that CTI is energy dependent. We choose to implement an energy dependent CTI correction as a broken power law with index  $\beta_1$  and  $\beta_2$  below and above the break energy:

$$\begin{aligned} CTI(E) &= CTI(E_{55\text{Fe}}) \left(\frac{E}{E_{55\text{Fe}}}\right)^{-\beta_1} & (E \leq E_{55\text{Fe}}) \\ &= CTI(E_{55\text{Fe}}) \left(\frac{E}{E_{55\text{Fe}}}\right)^{-\beta_2} & (E > E_{55\text{Fe}}) \end{aligned}$$

with  $E_{55\text{Fe}} = 5.895 \text{ keV}$  and  $\beta > 0$ .

The CTI energy dependence parameters in the CALDB gain files are labelled as BETA1, BETA2 and E\_CTI.

## A.7 Trap correction coefficients

The trap corrections are implemented in the gain files using an additive offset coefficient to equation A.12:

$$PI \times G = PHA(GC0 + X \times GC1 + Y \times GC2) + GC3 + X \times GC4 + Y \times GC5 + OFFSET \quad (\text{A.16})$$

The OFFSET coefficient is added to the  $PI \times G$  values of events detected at specific CCD locations affected by charge traps. In the gain files, the trap positions are labelled as RAWX, RAWY and YEXTENT, such that the OFFSET PI value will be added to events along the CCD column RAWX between rows RAWY and RAWY+YEXTENT.

The trap offset energy dependence is modelled with a broken power law, with the break at the reference energy of 1.856 keV (the energy of the Silicon  $K\alpha$  line of the Tycho SNR):

$$\begin{aligned} Offset(E) &= Offset(E_{break}) \left(\frac{E}{E_{break}}\right)^{\alpha_1} & (E \leq E_{break}) \\ &= Offset(E_{break}) \left(\frac{E}{E_{break}}\right)^{\alpha_2} & (E > E_{break}) \end{aligned}$$

The offsets energy dependence parameters in the CALDB gain files are labelled as ALPHA1, ALPHA2 and EBREAK. The gain and CTI coefficients and the energy dependence parameters used by the software to compute trap corrected events energy are labelled as GC0\_TRAP, GC1\_TRAP, GC2\_TRAP, GC3\_TRAP, GC4\_TRAP, GC5\_TRAP, BETA1\_TRAP, BETA2\_TRAP and E\_CTI\_TRAP.

## B Gain and CTI measurements

### B.1 Corner source data analysis

Gain and CTI coefficients are measured from the analysis of the corner source data. A first set of coefficients is derived using the entire dataset, and characterises the CCD response when trap energy corrections are not applied. A second set of coefficients, derived from corner source data least affected by traps, models the gain and the CTI of trap-corrected spectra. For both derivations, the same procedure is applied and is described below.

The corner source data have been reprocessed to ensure the latest photon counting mode bias corrections were applied, as this has previously been shown to correct the gain during the times of highest CCD operating temperatures (above  $-55^{\circ}\text{C}$ ) and is the default operation for the *Swift* software tools. Grade 0 PHA spectra were extracted from each of the corner sources as a function of time and CCD temperature. The spectra near the  $^{55}\text{Fe}$  line were then fit with the following asymmetric Gaussian function :

$$\begin{aligned} G(x) &= N \exp\left(-0.5 \left(\frac{x - x_c}{\sigma_1}\right)^2\right) && (x < x_c) \\ &= N \exp\left(-0.5 \left(\frac{x - x_c}{\sigma_2}\right)^2\right) && (x > x_c) \end{aligned}$$

where  $x_c$  is the line centre,  $\sigma_1$  the line width for  $x < x_c$ ,  $\sigma_2$  the line width for  $x > x_c$ , and  $N$  the normalisation. This models the line profile better and returns more accurate line centroids than a simple Gaussian, as the effect of CTI is to broaden the low energy line wing significantly more than the high energy line wing (Godet et al. 2009, A&A, 494, 775). Figure B.2 illustrates the measured line centroids, gain and CTI coefficients from 2007-Sep-05 to 2010-Sep-31 at a CCD temperature of  $-57^{\circ}\text{C}$  when all the corner source data is used (i.e., without excluding traps).

Due to the excellent quantity and statistical quality of the corner source data obtained since 2008-June we have been able to study and quantify the measured gain and CTI coefficients behaviour as a function of time and CCD temperature. Figure B.3 shows the gain (GC0) and CTI coefficients (GC1,2) derived from the entire corner source dataset, plotted as a function of CCD temperature at 4 representative epochs. The data reveal the gain has evolved to become less sensitive to the CCD temperature, while the parallel CTI decreases with increasing temperature and the serial CTI increases slightly with temperature.

We have parameterised the gain and CTI time ( $t$ ) and CCD temperature ( $T$ ) dependence using the following functional form :

$$z(t, T) = a + bt + cT + dt^2 + eT^2 + ftT.$$

The model curves are shown plotted with the data in figure B.3.

The parameterised GC0, GC1 and GC2 (see equation A.12) values derived from non trap-corrected data were then converted into a template gain file with coefficients calculated at monthly intervals and at three discrete temperatures ( $-73$ ,  $-60.5$ ,  $-48^{\circ}\text{C}$ ). The *Swift*-XRT software task XRTCALPI interpolates over time and temperature when applying the gain calculation to the event data.

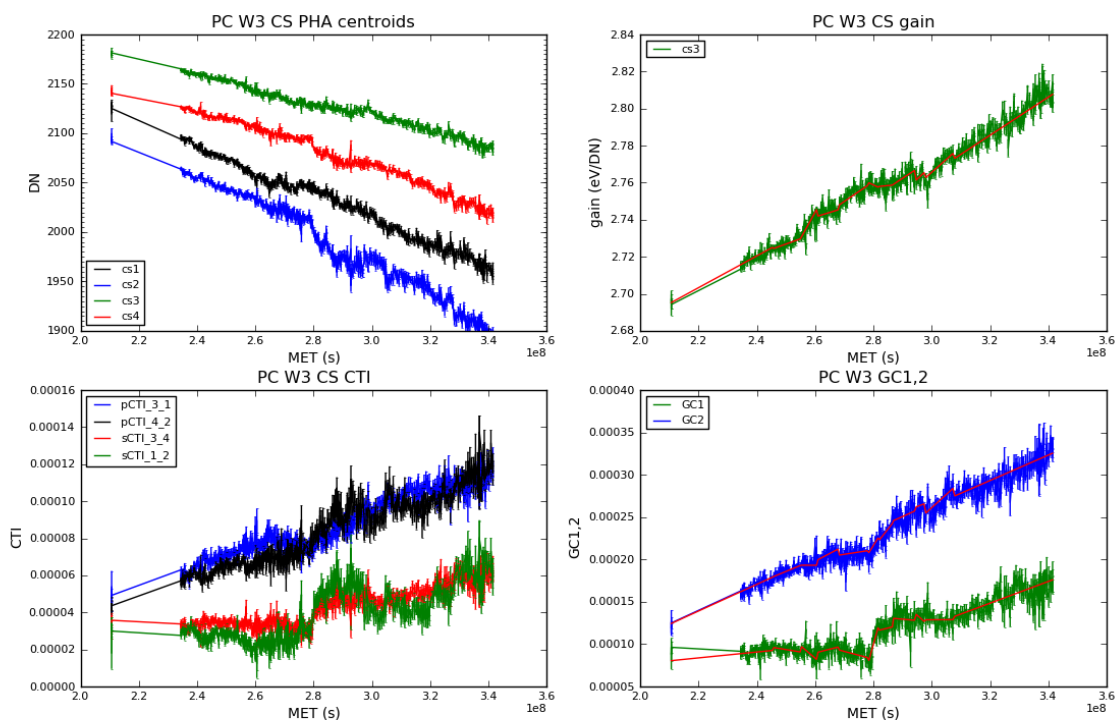


Figure B.2: *Swift*-XRT CCD gain and CTI measurements from the corner source data at a CCD temperature of  $-60^{\circ}\text{C}$  from 2007-Sep-05 to 2011-Oct-31. No trap-correction has been applied to the data. The top-left panel shows the measured  $^{55}\text{Fe}$  line centroids. The top-right panel shows the gain coefficient ( $GC0$ ) estimated using equation A.11. The bottom-left panel shows the measured CTI coefficients for the 4 pairs of corner sources. The bottom-right panel shows the estimated gain file  $GC1$  (serial) and  $GC2$  (parallel) coefficients. (Error bars are  $1\sigma$  estimates.)

The template gain file for non trap-corrected data was tested on various data sets which included the corner source data (PC mode) and the line rich SNRs E0102 and Cas A (both PC and WT mode). The low energy spectrum of SNR E0102, in particular, is sensitive to the presence of residual offsets in the energy scale. This is due to the presence of traps that causes energy offsets of the observed energies.

PC mode observations of E0102 taken during 2007-Sep-25 to 2007-Oct-02 and 2008-Oct-01 to 2008-Oct-04 revealed the need for an additional offset of 15 eV. A similar level of offset was obtained from PC mode observations of Cas A taken on 2007-Oct-05 and 2008-Sep-04.

At present, we have no independent measure of the CTI characterisation in WT mode so we use the PC mode CTI coefficients in the construction of the WT gain file. Like PC mode, we checked the residual offset using observations of E0102 taken in 2007-Sep-30 to 2007-Oct-01 and 2008-Aug-24 to 2008-Oct-09. These showed an average offset of 38 eV. The appropriate offsets measured above are included as the  $GC3$  coefficient in the gain files.

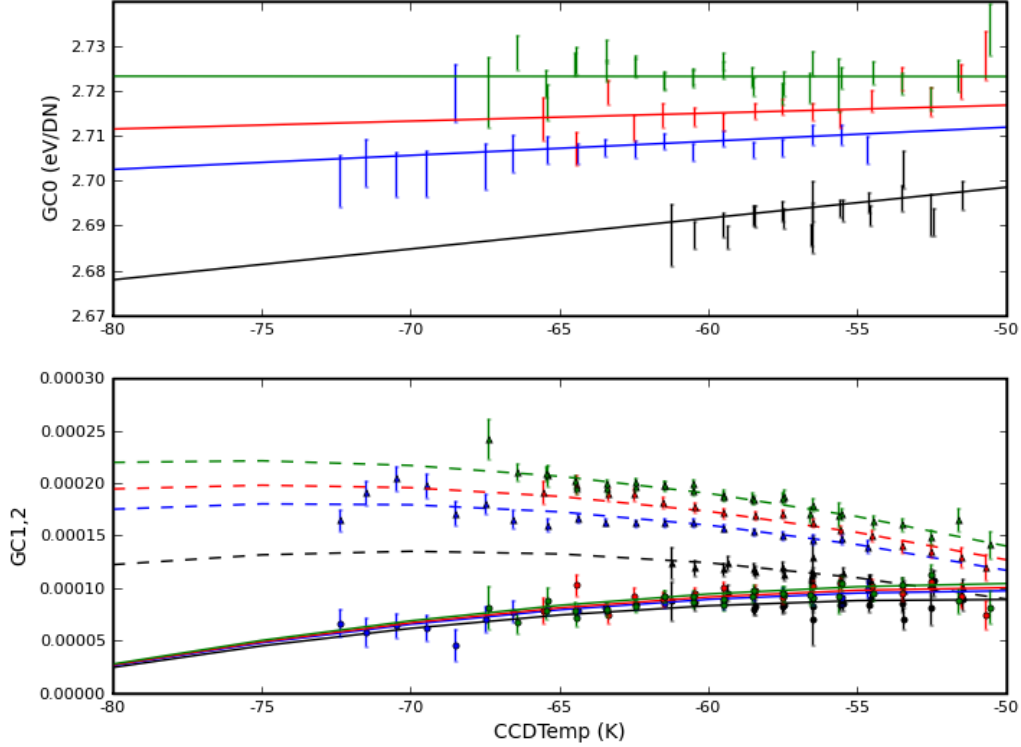


Figure B.3: *Swift*-XRT CCD gain (GC0) and CTI (GC1,2) coefficients plotted against CCD temperature. The model described in the text is over-plotted as the curved lines. For both panels the colour coding is as follows: black – 2007-Sep-06; blue – 2008-Jun-07; red – 2008-Sep-15; green – 2008-Jan-25. In the lower panel, the GC1 (serial) values are drawn as circles and the model is represented by the solid curves, while the GC2 (parallel) values are drawn as triangles and the model curves are shown dashed.

## B.2 Gain and CTI coefficients for trap-corrected spectra

The analysis of the corner source data have revealed an ever increasing number of deep traps (20 eV or deeper) in the XRT camera. Because these deep traps were not excluded from the corner source analysis, the gain and CTI coefficients measured as described above are representative of a CCD response with no trap corrections applied and are labelled in the gain files as GC0, GC1, GC2 and GC3.

To characterise the gain and the CTI of trap-corrected spectra the corner source columns least affected by traps were selected. In particular, the columns within 50 eV of the highest measured  $^{55}\text{Fe}$  energy centroid in the bottom left corner source (DETX = 13, 17, 22, 41) were used to derive the gain coefficient. For the parallel CTI, the accepted columns had a centroid difference in the top and the bottom corner sources within  $\pm 2$  PI channels ( $\pm 25$  eV) of each other: DETX = 6, 9, 13, 20, 23, 31, 36, 47, 57, 67, 68, 69 on the left side of the CCD; DETX = 539, 542, 548, 550, 558, 574, 578, 588, 596, 598 on the right side of the CCD. As already mentioned, the serial CTI for trap corrected spectra is set to zero in the CALDB files, as global energy offsets for each CCD column are instead measured and included in the gain file; for this same reason, GC3\_TRAP is also zero in the gain files.

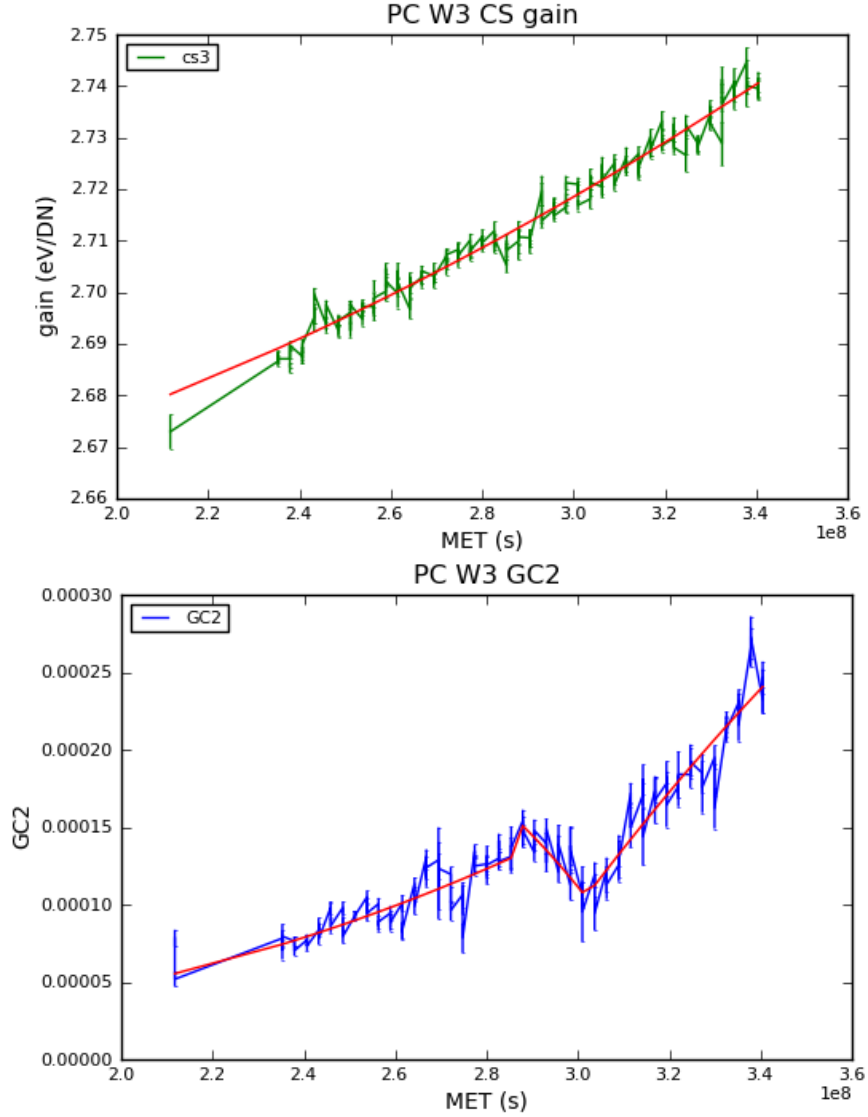


Figure B.4: Gain and parallel CTI coefficients from the subsample of events of the corner source data least affected by trap charge losses. These coefficients are used to derive the energy of events when the trap correction is applied by the the software task XRTCALPI.

The coefficients used by the software task XRTCALPI when the trap correction is applied are labelled as GC0\_TRAP, GC1\_TRAP, GC2\_TRAP and GC3\_TRAP (GC1\_TRAP and GC3\_TRAP are set to 0). The coefficients are parametrised as a function of time and CCD temperature with the same functional form used for the gain and CTI coefficients of uncorrected spectra previously described. The gain (GC0\_TRAP) and parallel CTI (GC2\_TRAP) measurements as a function of time at the CCD temperature of  $\sim 60C$  are shown in figure B.4.

## C Previous Releases

Table C.1: Previous gain file releases.

FILENAME	VALID DATE	RELEASE DATE	REVISION
swxpcgain20010101v003.fits	01-Jan-2001	15-Oct-2004	003
swxpdgain20010101v003.fits	01-Jan-2001	15-Oct-2004	003
swxwtgain20010101v003.fits	01-Jan-2001	15-Oct-2004	003
swxpcgain20010101v004.fits	01-Jan-2001	10-Jan-2005	004
swxpdgain20010101v004.fits	01-Jan-2001	10-Jan-2005	004
swxwtgain20010101v004.fits	01-Jan-2001	10-Jan-2005	004
swxpcgain20010101v005.fits	01-Jan-2001	12-Oct-2005	005
swxpdgain20010101v005.fits	01-Jan-2001	12-Oct-2005	005
swxwtgain20010101v005.fits	01-Jan-2001	12-Oct-2005	005
swxpcgain20010101v006.fits	01-Jan-2001	1-Dec-2005	006
swxpdgain20010101v006.fits	01-Jan-2001	1-Dec-2005	006
swxwtgain20010101v006.fits	01-Jan-2001	1-Dec-2005	006
swxpcgains0_20010101v007.fits	01-Jan-2001	30-Jul-2007	007
swxpcgains6_20010101v007.fits	01-Jan-2001	30-Jul-2007	007
swxpdgains0_20010101v007.fits	01-Jan-2001	30-Jul-2007	007
swxwtgains0_20010101v007.fits	01-Jan-2001	30-Jul-2007	007
swxwtgains6_20010101v007.fits	01-Jan-2001	30-Jul-2007	007
swxwtgains0_20010101v008.fits	01-Jan-2001	21-Apr-2008	008
swxwtgains6_20010101v008.fits	01-Jan-2001	21-Apr-2008	008
swxpcgains0_20010101v008.fits	01-Jan-2001	07-Apr-2009	009
swxwtgains0_20010101v009.fits	01-Jan-2001	07-Apr-2009	009
swxpdgains0_20010101v008.fits	01-Jan-2001	07-Apr-2009	009
swxpcgains6_20010101v008.fits	01-Jan-2001	07-Apr-2009	009
swxwtgains6_20010101v009.fits	01-Jan-2001	07-Apr-2009	009
swxpcgains6_20010101v009.fits	01-Jan-2001	01-Dec-2009	009
swxwtgains6_20010101v010.fits	01-Jan-2001	01-Dec-2009	009
swxpcgains0_20010101v009.fits	01-Jan-2001	07-Jun-2011	010
swxwtgains0_20010101v010.fits	01-Jan-2001	07-Jun-2011	010
swxpdgains0_20010101v009.fits	01-Jan-2001	07-Jun-2011	010
swxpcgains6_20010101v010.fits	01-Jan-2001	07-Jun-2011	010
swxwtgains6_20010101v011.fits	01-Jan-2001	07-Jun-2011	010

Table C.1 lists the gain files made available through previous releases of the *Swift*-XRT CALDB and are described in CALDB documents SWIFT-XRT-CALDB-04\_v10, SWIFT-XRT-CALDB-04\_v9, SWIFT-XRT-CALDB-04\_v8, SWIFT-XRT-CALDB-04\_v2 and SWIFT-XRT-CALDB-04.